Research Square

Preprints are preliminary reports that have not undergone peer review.
They should not be considered conclusive, used to inform clinical practice,
or referenced by the media as validated information.

Embryo-derived extracellular vesicles contribute to the uterine miRNA profile during early pregnancy in pigs: an integrative in vivo and in vitro study

David Gascon-Collado
Instituto Nacional de Investigación y Tecnología Agraria y Alimentaria
Carolina G Cabrera-Gomez
Instituto Nacional de Investigación y Tecnología Agraria y Alimentaria
Paula Blanco-Cueto
Instituto Nacional de Investigación y Tecnología Agraria y Alimentaria
Adelina Lopez-Jara
Universidad de Murcia
Manuela Garcia-Canovas
Universidad de Murcia
Maria A Gil
Universidad de Murcia
Cristina Cuello
Universidad de Murcia
Inmaculada Parrilla
Universidad de Murcia
Emilio A Martinez
Universidad de Murcia
Cristina A Martinez-Serrano
cristina.martinez@inia.csic.es

Instituto Nacional de Investigación y Tecnología Agraria y Alimentaria

Research Article

Keywords: extracellular vesicles, embryo-maternal communication, microRNAs, embryo-derived extracellular vesicles, uterine fluid, early pregnancy, blastocyst, small RNA sequencing

Posted Date: November 19th, 2026

DOI: https://doi.org/10.21203/rs.3.rs-11554635/v1

License: This work is licensed under a Creative Commons Attribution 4.0 International License.
Read Full License

Additional Declarations: No competing interests reported.

Abstract

Background

Extracellular vesicles (EVs) are increasingly recognized as important mediators of intercellular communication at the embryo-maternal interface through the transfer of regulatory molecules, including microRNAs (miRNAs). However, the contribution of embryo-derived EVs to the uterine environment during early porcine pregnancy remains poorly understood. This study aimed to characterize EV-associated miRNA profiles from day-6 uterine fluid of pregnant (UF-P) and cyclic non-pregnant sows (UF-C), together with EVs released by *in vivo*-derived blastocysts (BL), to investigate the potential maternal and embryonic contributions to EV-mediated communication during early pregnancy.

Results

A total of 158 EV-associated miRNAs were identified across uterine fluid from pregnant (UF-P) and cyclic control sows (UF-C) and blastocyst-conditioned medium (BL). Of these, 95 miRNAs were shared among all three groups, whereas 31 were classified as maternal-associated, 3 as embryonic-associated, and 16 as interaction-associated based on their distribution across EV populations. Functional enrichment and target convergence analyses linked these miRNA signatures to pathways involved in Wnt, TGF-β, PI3K, FGF, PDGF, integrin, angiogenic, inflammatory, and apoptotic signaling. Global miRNA profiling further revealed distinct EV cargo patterns among UF-P, UF-C, and BL samples. Analysis of EVs released by in vitro-produced embryos provided additional support for an embryonic contribution to the identified signatures: miR-132-3p reads were consistently recovered from IVP-derived EVs, while miR-142-5p was detected at lower levels and miR-383-3p was predominantly associated with EVs released by in vivo-derived embryos.

Conclusions

These findings demonstrate that the uterine EV-associated miRNA landscape during early porcine pregnancy comprises distinct maternal and embryonic signatures. The results provide evidence that the embryo contributes to the uterine EV-miRNA pool before maternal recognition of pregnancy and suggest that EV-associated miRNAs participate in the molecular dialogue between the conceptus and the maternal reproductive tract.

1. Introduction

Successful pregnancy establishment requires a highly coordinated molecular dialogue between the developing conceptus and the maternal reproductive tract [1]. During the preimplantation period, the embryo undergoes a series of tightly regulated developmental events while simultaneously interacting with the uterine environment to ensure its survival and developmental progression [2]. Failure to

establish this bidirectional communication accounts for a substantial proportion of embryonic losses across mammalian species, highlighting the critical importance of embryo-maternal signaling during early pregnancy.

In this regard, the pig constitutes a valuable large-animal model for studying early embryo development and embryo-maternal communication in biomedicine, while also being of major importance for animal production [3, 4]. Improving our understanding of the mechanisms regulating embryo-maternal communication has direct implications for both livestock reproductive technologies and human assisted reproduction, particularly considering that the preimplantation period remains one of the most critical stages for embryonic survival. Despite its biological and clinical relevance, the molecular mechanisms governing this communication remain incompletely understood.

Extracellular vesicles (EVs) have emerged as evolutionarily conserved mediators of intercellular communication in virtually all biological systems. These membrane-enclosed particles are secreted by most cell types and transport a complex cargo of proteins, lipids, metabolites and nucleic acids that can modulate the physiology and gene expression of recipient cells [5]. By enabling the transfer of regulatory molecules between cells and tissues, EVs participate in a wide range of physiological processes, including immune regulation, tissue homeostasis, development, and disease. In reproductive biology, EV-mediated communication has been implicated in multiple processes ranging from gamete maturation and fertilization to embryo development and implantation [6, 7]. Increasing evidence indicates that EVs present in the oviductal and uterine fluids contribute to the establishment of a physiological environment that supports preimplantation embryo development [8]. In particular, uterine fluid (UF)-derived EVs have been shown to influence embryo quality, developmental competence and implantation-associated processes in bovine embryo culture [9]. In addition, embryo-derived EVs have been characterized in several species, including cattle [10, 11, 12], mice [13, 14], humans [15], sheep [16], among others.

A previous study reported the release of EVs by porcine embryos into the culture media [17]. However, this study used parthenogenetic embryos. Recently, our group demonstrated for the first time that *in vitro*-fertilized porcine embryos release EVs carrying distinct miRNA profiles associated with developmental competence [18]. However, the contribution of EVs released by *in vivo*-derived porcine embryos to the uterine EV-associated miRNA pool during early pregnancy remains unknown.

Among EV cargo molecules, microRNAs (miRNAs) are particularly attractive candidates for studying embryo-maternal communication because of their stability and their ability to coordinately regulate multiple target genes and biological pathways. Several uterine EV-associated miRNAs have been linked to implantation-related processes. In the pig, miR-26a and miR-125b have been identified in uterine EVs [19, 20], while more recent studies have demonstrated that EV-mediated transfer of miR-92b-3p and miR-143-3p regulates trophoblast proliferation, migration and adhesion, providing direct evidence that uterine EV-associated miRNAs can modulate processes relevant to implantation [21, 22].

Therefore, the aim of the present study was to characterize the EV-associated miRNA profiles of uterine fluid from pregnant and non-pregnant sows together with EVs released by *in vivo*-derived porcine

embryos. By integrating maternal and embryonic EV-associated molecular signatures, we sought to identify candidate regulatory molecules potentially involved in embryo-maternal communication during early pregnancy and to provide the first characterization of EVs released by *in vivo*-derived porcine embryos.

2. Material and Methods

2.1 Experimental design

In the present study, three main EV populations were analyzed. EVs were isolated from uterine fluid (UF) collected on day 6 from pregnant sows (UF-P, n = 5) and cyclic non-pregnant control sows (UF-C, n = 4). All sows underwent the same estrus synchronization and superovulation protocol. UF-P sows were artificially inseminated, whereas UF-C sows underwent post-cervical administration of extender without spermatozoa. Pregnancy status was confirmed at sample collection by the recovery of embryos from UF-P sows and the absence of embryos in UF-C sows. In addition, EVs were isolated from blastocyst-conditioned medium (BL, n = 5). A total of 250 *in vivo*-derived (IVD) day-6 blastocysts were recovered from 10 donor sows, including the 5 sows contributing to the UF-P group. Blastocysts from all 10 donor sows were distributed as evenly as possible among 5 pools of 50 embryos, thereby balancing donor contribution across BL replicates; each pool constituted one BL biological replicate. Before EV collection, embryos were washed 3 times in 1 mL of protein-free medium (NCSU-23), to minimize carryover from the uterine environment. Groups of 50 embryos were then incubated for 6 h in 500 µL of fresh protein-free NCSU-23 medium at 38.5°C under 5% CO_2 and saturated humidity. At the end of the incubation period, embryos were removed and the conditioned medium was immediately processed for EV isolation. EVs were isolated, characterized and subjected to small RNA-Sequencing. Based on the distribution of detected miRNAs across these three populations, miRNAs present in both UF-P and UF-C but absent from BL were classified as maternal-associated, whereas miRNAs detected in UF-P and BL but absent from UF-C were classified as embryonic-associated. miRNAs detected exclusively in UF-P, but absent in UF-C and BL groups, were operationally classified as interaction-induced, as their presence was restricted to the *in vivo* environment in which maternal tissues and embryos coexist. To provide additional evidence for the embryonic origin of the miRNAs classified as embryonic-associated, EVs released by groups of 50 *in vitro*-produced (IVP, n = 5) embryos, cultured for 6 h in protein-free medium, were also analyzed. A schematic representation of the experimental design is shown in Fig. 1.

2.2 Animals and farm management

This study was conducted under field conditions at a commercial pig farm located in southeastern Spain (Agropor SA, Murcia, Spain). Adult crossbred sows (Landrace × Large White) from the same genetic line, with parities ranging from 1 to 5 and a lactation period of 21–24 days, were selected. Following weaning, sows were randomly assigned to the experiment. The sows were housed individually in crates within a mechanically ventilated confinement facility. Semen donors were sexually mature boars (2–3 years of age) of proven fertility, kept in individual pens under climate-controlled conditions at a commercial

artificial insemination center in Murcia (Spain). All animals had ad libitum access to water and were fed commercial diets according to their nutritional requirements.

2.3 Estrus synchronization and artificial insemination

Estrus was synchronized by weaning. Sows were superovulated following a hormonal protocol: on day 1 after weaning, each sow received 1,000 IU of equine chorionic gonadotropin (eCG; Foligon®, Intervet). Only sows with a weaning-to-estrus interval of 3–4 days were included in the study. Starting two days after weaning, estrus was monitored once daily by trained staff. Detection involved snout-to-snout contact with a mature boar and manual back-pressure testing. Sows exhibiting the standing reflex were considered in estrus and selected for the experimental procedures. Only sows with clear signs of estrus at 48–72 h post-eCG administration were further intramuscularly administered with 750 IU of human chorionic gonadotropin (Veterin Corion, Divasa, Farmavic S.A., Barcelona, Spain) at the onset of estrus. Post-cervical inseminations were performed at 0, 24, and 36 h after estrus onset.

2.4 UF and embryo collection

Uterine fluid and embryos were collected by laparotomy. All surgical procedures were performed in an on-farm operating room. On day 6 of the estrus cycle (day 0 = estrus onset), sows underwent a mid-ventral laparotomy. Sedation was induced with intramuscular azaperone (2 mg/kg body weight), followed by intravenous sodium thiopental (7 mg/kg body weight) and anesthesia was maintained using 3–5% isoflurane. The reproductive tract was exposed, and UF was collected as follows: a small incision was made in the uterine wall approximately 20 cm distal to the utero-tubal junction using blunt Adson forceps, and a glass cannula was inserted through this opening. A total of 30 mL of a protein-free flushing medium, based on Tyrode's lactate (TL) HEPES-polyvinyl alcohol (PVA) with slight modifications [23], was infused into the cranial end of each uterine horn. The recovered fluid from both horns was pooled for each sow. Embryos collected along with UF were examined under a stereoscope (60× magnification) to allow stage classification. Samples were immediately placed in a portable heating unit at 38.5°C and transported to the laboratory for further processing.

2.5 In vitro embryo production

Ovaries were obtained from prepubertal crossbred gilts at a commercial abattoir (Comarán, S.L., Madrid, Spain) and transported to the laboratory at 33°C in saline solution (9 mg/mL NaCl) supplemented with kanamycin (70 µg/mL). Follicles measuring 3–7 mm in diameter were opened with a sterile scalpel in TL-HEPES medium supplemented with 0.01% PVA. Only cumulus-oocyte complexes (COCs) surrounded by at least three compact layers of cumulus cells were selected for *in vitro* maturation (IVM). Groups of 70 COCs were cultured in four-well dishes containing 500 µL of TCM-199 maturation medium supplemented with 10 IU/mL equine chorionic gonadotropin (eCG) and 10 IU/mL human chorionic gonadotropin (hCG) for the first 22 h. COCs were then transferred to the same medium without hormonal supplementation for an additional 22 h. After 44 h of IVM, cumulus cells were removed by vortexing the COCs for 2 min at 1400 rpm in TL-HEPES-PVA supplemented with 0.1 mg/mL hyaluronidase. Denuded oocytes were washed 3 times in maturation medium and subsequently in *in vitro*-fertilization (IVF)

medium, consisting of Tris-buffered medium supplemented with 2 mM caffeine and 0.2 mg/mL bovine serum albumin (BSA). Groups of 35–40 oocytes were placed in 50-µL droplets of IVF medium and inseminated with frozen-thawed spermatozoa prepared as previously described by Gil et al. [24]. Briefly, one semen straw was thawed at 37°C for 20 s, and 200 µL of sperm suspension was washed three times in Dulbecco's phosphate-buffered saline containing 4% BSA by centrifugation at 1900 × g for 3 min. The resulting sperm pellet was resuspended in IVF medium to achieve a final sperm-to-oocyte ratio of 1000:1. Subsequently, 50 µL of sperm suspension was added to each oocyte-containing droplet, and gametes were co-incubated for 5 h. Following IVF, presumptive zygotes were washed by repeated pipetting in *in vitro* culture (IVC) medium to remove residual spermatozoa attached to the zona pellucida. Embryos were cultured in groups of 40 in four-well dishes containing 500 µL of an NCSU-based medium supplemented with 0.3 mg/mL PVA and 0.4% BSA. During the first 2 days of IVC, the medium was additionally supplemented with 0.3 mM pyruvate and 4.5 mM lactate. Thereafter, embryos were transferred to fresh IVC medium supplemented with 5.5 mM glucose and maintained for an additional 5 days. On day 5 of culture, fetal bovine serum was added to a final concentration of 10%. All culture steps were performed under paraffin oil at 38.5°C in a humidified atmosphere of 5% CO_2 in air.

2.6 EV Isolation and characterization

Samples were centrifuged at 300 × g for 7 min at 4°C to remove intact cells and large debris. The supernatant was then centrifuged at 10,000 × g for 30 min at 4 ºC to remove residual cellular debris, and filtered through 0.22 µm syringe filters (Millex® syringe filters, Darmstadt, Germany). EV isolation was performed using size-exclusion chromatography with PURE-EVs® columns (HansaBioMed Life Sciences, Tallinn, Estonia). Isolation was carried out according to the manufacturer's instructions. Briefly, columns were washed with 30 mL of phosphate-buffered saline (PBS), after which 2 mL of each sample were loaded onto the column. The EV-enriched fraction (2.5 mL) was collected as the fraction of interest. The EV-rich fraction was subsequently concentrated using ultrafiltration (Pierce Protein Concentrator, PES membrane, 100 kDa MWCO, Waltham, USA) by centrifugation at 3,500 × g for 10 min at room temperature. Concentrated EVs samples were stored at 4 ºC, -20 ºC or -80°C depending on the downstream analysis.

The isolated EVs were characterized in accordance with the Minimal Information for Studies of Extracellular Vesicles (MISEV2023) guidelines [25]. Particle size distribution and zeta potential were analyzed by dynamic light scattering (DLS), using a Zetasizer Nano ZS system (Malvern Panalytical, Malvern, UK), operating at 633 nm and detecting backscattered light at 173° at room temperature. Before analysis, EV samples were gently agitated at 50 rpm for 30 s to minimize particle aggregation. Samples were loaded into 10-mm pathlength cuvettes (50 µL) for particle size measurements or disposable folded capillary cells (750 µL) for zeta-potential analysis. Light scattering was recorded for 150 s, with three measurements performed per sample for particle size distribution and one measurement for zeta potential. Measurements were conducted at 25°C after a 60-s equilibration period, using a refractive index of 1.33 and an absorption coefficient of 0.01. Data were acquired and processed using Dispersion

Technology Software v.5.10 (Malvern Panalytical). Particle size distributions were intensity-weighted and expressed as the 25th -75th percentile range.

EV morphology was assessed by cryo-electron microscopy (cryo-EM) and transmission electron microscopy (TEM) at the Electron Microscopy Facility of the National Center for Biotechnology (CNB-CSIC, Madrid, Spain). For cryo-EM analysis, EV samples were applied onto glow-discharged holey carbon grids, blotted to remove excess liquid, rapidly vitrified in liquid ethane, and imaged under low-dose conditions to preserve vesicle structure in a near-native hydrated state. For TEM analysis, 10 µL of EV suspension per sample were applied onto electron microscopy grids, negatively stained following standard protocols, and examined under appropriate accelerating-voltage conditions.

EV immunophenotyping was performed by high-resolution flow cytometry using a CytoFLEX S cytometer (Beckman Coulter) equipped with 405-, 488-, 561-, and 638-nm lasers. Side-scatter (SSC) detection was configured using the 405-nm laser (violet SSC). EV preparations were analyzed in separate aliquots using CellTrace™ CFSE (Thermo Fisher Scientific) for EV-associated fluorescence and antibodies against the EV markers CD9 (PerCP-conjugated), CD63 (FITC-conjugated), and CD81 (APC-conjugated), as well as albumin-FITC as a purity-associated marker. FITC, PerCP, and APC fluorescence were collected through 525/25-, 710/30-, and 670/40-nm filters, respectively. EV events were identified using a polygonal gate based on violet SSC and forward scatter (FSC) parameters. Marker-positive events were quantified in the corresponding antibody-stained aliquots and expressed relative to the EV event population defined using the same scatter-gating strategy. Appropriate reagent and fluorescence controls were used to establish background signals and positivity thresholds.

2.7 RNA extraction and small RNA sequencing

Total RNA was isolated using the miRNeasy Tissue/Cells Advanced Micro kit (QIAGEN GmbH, Hilden, Germany) according to the manufacturer´s instructions. RNA concentration and quality were evaluated by Qubit™ 4 Fluorometer (Thermo Fisher Scientific) using the Qubit™ microRNA Assay Kit (Thermo Fisher Scientific, Oregon, USA). For EV-associated miRNA profiling, purified RNA samples were sent to Dreamgenics (Asturias, Spain) for library preparation and sequencing. RNA integrity and quality were first assessed using an Agilent 2100 Bioanalyzer (Agilent Technologies, Santa Clara, CA, USA). Small RNA libraries were prepared from 10 ng of total RNA using the NEBNext Small RNA-Library Prep Set (New England Biolabs, Ipswich, MA, USA), following the manufacturer’s recommendations. Adapter sequences were ligated to the 3' and 5' ends of the RNA molecules, followed by reverse transcription and polymerase chain reaction (PCR) amplification to generate double-stranded cDNA libraries. Libraries were subsequently purified and size-selected to retain inserts corresponding to small RNAs of approximately 18–40 nucleotides. Library concentration and quality were evaluated by Qubit fluorometry, quantitative PCR and the Agilent 2100 Bioanalyzer. Equimolar libraries were then pooled and sequenced on an Illumina NovaSeq 6000 platform using a single-end 50-bp sequencing strategy.

2.8 Bioinformatic analysis

Raw sequencing reads were processed using Partek Flow software (Partek, St. Louis, MO, USA). Adapter trimming and quality filtering were performed prior to alignment. Clean reads were aligned to the *Sus scrofa* reference genome (Sscrofa11.1) using the Bowtie algorithm implemented in Partek Flow, and alignment quality was assessed based on mapping statistics. Aligned reads were quantified against the *Sus scrofa* reference annotation (Ensembl release 115, Sscrofa11.1), and low-expression features were filtered to reduce background noise. Differential miRNA abundance was analyzed using the DESeq2 algorithm implemented in Partek Flow. Pairwise comparisons were performed using a nominal P value < 0.05 and an absolute fold-change (FC) > 1.5 as thresholds for differential abundance. Benjamini-Hochberg false discovery rate (FDR) correction was additionally applied to identify miRNAs remaining significant after multiple-testing correction. Principal component analysis (PCA) and hierarchical clustering were performed in Partek Flow to evaluate global differences among experimental groups.

2.9 Target prediction and functional enrichment analysis

For qualitative miRNA profiling, miRNAs were considered reliably detected in an experimental group when they exhibited at least 10 raw counts in a minimum of 50% of the biological samples within that group. To investigate the potential biological functions of the group-specific EV-associated miRNAs, porcine miRNA precursors identified by small RNA-sequencing were first mapped to their corresponding mature miRNAs. The Integrative Genomics Viewer (IGV) [26] was used to visualize sequencing read alignments and determine whether the detected mature miRNAs corresponded to the 3p or 5p arm of their respective precursors. Functional annotation of the mature miRNA sets was performed using miEAA 2.1 (miRNA Enrichment Analysis and Annotation) [27]. Over-representation analysis was conducted using Gene Ontology (GO) Biological Process annotations. Enrichment significance was assessed using Fisher's exact test and corrected for multiple testing using the Benjamini-Hochberg procedure. GO terms with an adjusted P value (FDR) < 0.05 were considered significantly enriched. For target prediction, the corresponding human homologue of each mature porcine miRNA was identified using miRbase [28] to retrieve and compare mature miRNA sequences between Sus scrofa and Homo sapiens and sequence conservation was assessed, with particular consideration of the seed region (nucleotides 2–8), which is the primary determinant of miRNA target recognition. Only mature porcine miRNAs with a conserved human homologue and an identical seed sequence were retained for downstream analysis. Predicted target genes for the corresponding human miRNAs were subsequently retrieved using TargetScanHuman [29]. Only transcripts containing conserved target sites and showing a cumulative weighted context + + score ≤ − 0.10 were retained for downstream analyses, with more negative scores indicating a stronger predicted regulatory effect. The resulting target genes were further subjected to functional enrichment analysis to identify biological processes and signalling pathways potentially regulated by the group-specific EV-associated miRNAs using PANTHER and STRING tools [30, 31].

3. Results

3.1. Characterization of EVs

DLS revealed that EVs isolated from the UF-P, UF-C and BL groups displayed particle size distributions consistent with small EVs (Fig. 2A). Median particle diameters ranged from 99.7 to 124.1 nm among the three groups. The predominant particle populations were centred at approximately 94–104 nm, accounting for the majority of detected particles in each preparation. EVs isolated from BL samples exhibited a more homogeneous size distribution, whereas UF-derived EVs showed additional minor populations of larger particles. Electron microscopy analyses confirmed the presence of membrane-bound vesicles in all groups, showing predominantly spherical vesicles with well-defined lipid bilayers and heterogeneous sizes, consistent with the characteristics of small EVs (Fig. 2B). Flow cytometry analysis further supported the EV-enriched nature of the isolated fractions through the detection of the canonical tetraspanin markers CD81, CD63 and CD9. CD81 was the most abundant EV-associated marker, being detected in approximately 60–64% of CFSE-positive particles across groups, whereas lower proportions of CD63- (approximately 8–10%) and CD9-positive particles (approximately 8–10%) were observed. In contrast, albumin-positive particles represented less than 6% of the CFSE-positive population, consistent with a low contribution of albumin-associated contaminants to the isolated EV fractions (Fig. 2C–D).

3.2. EV-associated miRNA distribution reveals maternal-, embryonic- and interaction-induced profiles

A total of 158 miRNAs were detected across EVs isolated from UF-P, UF-C, and BL. Most miRNAs (95/158; 60.1%) were detected in all three EV populations (Fig. 3A). However, comparison of miRNA distribution among groups also revealed distinct patterns potentially associated with maternal and embryonic contributions to the UF EV-miRNA pool. 31 miRNAs (19.6%) were detected in both UF-P and UF-C but were absent from BL EVs and were therefore classified as maternal-associated miRNAs. Conversely, 3 miRNAs (1.9%) were shared between UF-P and BL but were absent from UF-C and were classified as embryonic-associated miRNAs. Notably, 16 miRNAs (10.1%) were exclusively detected in UF-P EVs and were absent from both UF-C and BL EVs. As these miRNAs were detected only in the uterine environment in which the maternal tract and embryos coexist, they were classified as interaction-induced miRNAs (Fig. 3A,B). Functional enrichment analysis further indicated that the 3 miRNA profiles were associated with distinct biological processes (Fig. 3C). Maternal-associated miRNAs were enriched in processes related to immune regulation, morphogenesis, cell-cell adhesion and angiogenesis. Embryonic-associated miRNAs were associated with processes including endothelial cell adhesion and migration, innate immune regulation, Rac signalling, and blood vessel development. Interaction-induced miRNAs showed enrichment in processes related to chromatin regulation, actin organization, β-catenin regulation, cellular stress responses and apoptosis, among others.

3.3. Predicted target convergence reveals distinct and shared regulatory pathways of maternal- and embryonic-associated miRNAs

To further investigate the potential regulatory functions of the maternal- and embryonic-associated miRNA profiles, predicted target genes were identified using TargetScan and subsequently examined for target convergence (Fig. 4A,B, Additional files 1&2). Target prediction for 10 selected maternal-associated miRNAs and 3 embryonic-associated miRNAs identified 4220 and 2182 unique target genes, respectively. Of these, 1295 maternal-associated and 83 embryonic-associated genes were predicted to be targeted by at least two miRNAs, and were used for pathway analyses. Pathway analysis of these convergent targets revealed both shared and group-specific biological functions (Fig. 4C). Maternal-associated targets were broadly represented in pathways involved in GnRH receptor signaling, Wnt signaling, inflammatory chemokine and cytokine signaling, integrin signaling, angiogenesis, growth-factor signaling, TGF-β signaling, apoptosis, PI3K signaling, p53 signaling, and interleukin signaling. Several of these pathways were significantly overrepresented after FDR correction, including Wnt, GnRH receptor, integrin, angiogenesis, PDGF, EGF, FGF, TGF-β, PI3K, insulin/IGF, interleukin, apoptosis, p53, and inflammatory signaling pathways. Embryonic-associated convergent targets were also represented in several pathways identified in the maternal signature, including GnRH receptor, Wnt, inflammatory signaling, integrin, CCKR, angiogenesis, EGF, FGF, TGF-β, interleukin, and p53 signaling, although the number of predicted target genes assigned to these pathways was substantially lower. Additional embryonic-associated targets mapped to Ras signaling, p53 feedback regulation, and angiotensin II signaling.

3.4. Interaction-induced miRNAs show extensive target convergence and enrichment in signaling pathways related to embryo-maternal communication

To further investigate the potential biological relevance of the miRNAs exclusively detected in UF-P EVs, but absent in UF-C and BL, target prediction analysis was performed for the interaction-induced miRNA group (Fig. 5A, Additional file 3). Target prediction for 10 selected miRNAs collectively yielded 4,819 unique predicted target genes. Of these, 1,023 genes were predicted to be targeted by at least two miRNAs, and were further analyzed. Pathway analysis of the convergent target genes revealed a broad representation of signaling pathways associated with developmental regulation, cell survival, and immune communication (Fig. 5B). The most represented pathways included Wnt signaling, GnRH receptor signaling, TGF-β signaling, PDGF signaling, apoptosis signaling, interleukin signaling, chemokine/cytokine-mediated inflammation, CCKR signaling, FGF signaling, and angiogenesis, among others. Enrichment analysis further showed that several of these pathways were significantly overrepresented (Fig. 5C), such as PI3 kinase, interleukin, apoptosis, PDGF, p53, FGF, Wnt, and GnRH receptor signaling pathways. To explore the relationships among convergent target genes (genes targeted by ≥ 3 miRNAs), an interaction network was generated (Fig. 5D). This network revealed a highly interconnected set of genes, including *PIK3CB, AKT3, PTEN, TGFB2, TGFBR1, LIF, IL6R, CREB1, MAPK1* and *FOS*, among others.

3.5 Differential miRNA profiles among groups

Global miRNA profiling revealed distinct expression patterns among the three groups. PCA showed a clear separation of UF-P, UF-C and BL samples, consistent with their distinct miRNA cargo profiles (Fig. 6A). Hierarchical clustering of miRNAs meeting both FDR < 0.05 and |FC| > 1.5 illustrated the group-specific expression patterns across individual samples (Fig. 6B). Pairwise differential expression analysis further revealed marked differences among EV populations. Using thresholds of P < 0.05 and |FC| > 1.5, 17 miRNAs were differentially expressed between UF-P and UF-C (5 upregulated and 12 downregulated in UF-P), 44 between UF-P and BL (22 upregulated and 22 downregulated in UF-P), and 47 between UF-C and BL (24 upregulated and 23 downregulated in UF-C) (Fig. 6C-E). The most pronounced changes (|FC| > 3) are highlighted in the volcano plots, while miRNAs remaining significant after multiple-testing correction (FDR < 0.05) are summarized below each comparison.

3.6 Pathway analysis of differentially abundant EV-associated miRNAs targets

To identify signaling pathways potentially affected by the differentially abundant EV-associated miRNAs, predicted target genes were classified according to Panther Pathways. Across the three comparisons, several recurrent signaling pathways associated with cell communication, proliferation, survival, adhesion, vascular regulation and immune responses were represented, including Wnt, TGF-β, PI3K, MAPK, FGF, EGF, PDGF, integrin, angiogenesis and inflammatory signaling pathways (Fig. 7). In the UF-P vs UF-C comparison, pathway overrepresentation analysis identified seven significantly enriched pathways (FDR < 0.05), including p38 MAPK signaling, cytoskeletal regulation by Rho GTPase, Gq/Go- and Gi/Gs-mediated G-protein signaling, CCKR signaling, integrin signaling and GnRH receptor signaling. In the UF-P vs BL comparison, significant overrepresentation was more restricted, with enrichment of the Insulin/IGF-AKT signaling cascade and CCKR signaling. Finally, the UF-C vs BL comparison showed significant enrichment of GnRH receptor, integrin, Gi/Gs-mediated G-protein and Wnt signaling pathways. Overall, the recurrence of developmental, adhesion and signaling pathways across comparisons indicates that differences in EV-associated miRNA profiles are linked to distinct regulatory landscapes in cyclic UF, pregnant uterine fluid and blastocyst-derived EVs.

3.7 Validation of embryonic-associated miRNAs in EVs released by IVP-embryos

EVs released by IVP-embryos were first characterized to confirm the presence of vesicular structures in the conditioned medium (Fig. 8A-C). To further validate the capacity of embryos to release the three miRNAs classified as embryonic-associated, miR-132-3p, miR-142-5p and miR-383-5p were subsequently examined in EVs released by IVP embryos and compared with EVs released by IVD-blastocysts (Fig. 8D). miR-132-3p was detected in all IVP replicates, providing strong evidence that this miRNA can be released by the embryo independently of previous exposure to the maternal reproductive tract. miR-142-5p was also detected in four of five IVP replicates, further supporting its embryonic expression and release, although raw read counts were lower than those observed in IVD embryo-derived

EVs. In contrast, miR-383-5p was undetectable in IVP-derived EVs, with only one read detected in two samples, whereas it was readily detected in three of five IVD samples.

4. Discussion

The present study provides new insights into EV-associated miRNA signaling between the embryo and the maternal tract during the earliest stages of porcine pregnancy. UF EVs inevitably contain particles released from multiple tissues and cell types, making their biological origin difficult to resolve when the UF is studied in isolation. In this study, we show that the embryo also contributes to the uterine EV-associated miRNA pool. More importantly, we identified a distinct miRNA profile that was detected only when the embryo and the maternal tract coexisted *in vivo*.

A substantial proportion of the detected miRNAs was common to all three groups, with 95 of 158 miRNAs shared among UF-P, UF-C and BL groups, reflecting a core EV-associated miRNA repertoire used by both embryonic and maternal sides. However, the distribution analysis revealed clearly distinguishable molecular profiles, where 31 miRNAs were detected in both UF-P and UF-C but not in BL-derived EVs, a pattern consistent with a predominantly maternal contribution. Conversely, only 3 miRNAs were detected in both BL-derived EVs and UF-P but were absent from UF-C, providing evidence that the embryo contributes to the EV pool found in the uterine fluid.

The maternal-associated miRNA signature may be particularly relevant in the context of uterine preparation for pregnancy establishment. In pigs, the classical maternal recognition of pregnancy occurs around days 11–13, when conceptus-derived estrogens redirect endometrial prostaglandin secretion and initiate a series of changes that precede conceptus attachment [32]. Importantly, however, acquisition of uterine receptivity begins before this period and involves progesterone-dependent remodeling of the endometrium, changes in cytokine and growth-factor signaling, and preparation of the epithelial surface for subsequent conceptus attachment [33, 34].

We paid particular attention to 10 maternal-associated miRNAs linked to pregnancy-related processes (miR-30b, miR-96, miR-150, miR-130b, miR-133a, miR-181c, miR-223, miR-214, miR-149 and miR-429). Several of these miRNAs have previously been associated with the porcine maternal-conceptus interface. In particular, miR-181 family members were experimentally shown to interact with the 3'UTRs of *SPP1, ITGB3* and *ESR1*, genes with well-established roles in conceptus attachment, integrin-mediated adhesion and estrogen-responsive uterine signaling [35]. Importantly, some of the maternal-associated miRNAs identified here have also been detected directly in porcine uterine EVs. miR-30b-5p was among the highly abundant miRNAs carried by uterine EVs during the peri-implantation period and was predicted to target transcripts that were subsequently downregulated in trophoblast cells following EV uptake, supporting its potential contribution to EV-mediated maternal-conceptus communication [36]. Recurrently predicted targets included genes linked to TGF-β, PDGF, PI3K, FGF, integrin/cytoskeletal and angiogenic signaling, including *TGFBR1, PDGFRA, PIK3C2A, FRS2, RAP1B, WASL* and *ERG*. These pathways are highly relevant to pregnancy establishment in pigs [3, 33, 37, 38]. TGF-β ligands and their

receptors increase at the porcine conceptus-maternal interface during the peri-implantation period, and active TGF-β/TGFBR signaling has been implicated in integrin-associated conceptus attachment [39, 40]. Similarly, FGF7 is produced by the uterine luminal epithelium and acts through FGFR2 expressed in both uterine epithelia and conceptus trophectoderm, supporting proliferation and differentiation during conceptus development and implantation [41]. PDGF receptors are also present in porcine endometrial stromal and endothelial cells and show strong immunoreactivity during early pregnancy, consistent with a role in tissue and vascular remodeling [42].

On the other hand, the roles of the embryonic-associated miRNAs (especially miR-132 and miR-142), further support their potential involvement in early embryo-maternal signaling. miR-132 has previously been reported as the only differentially expressed miRNA between pregnant and cyclic porcine endometrium on day 12, and lncRNA-miR-132-mRNA interactions were proposed to contribute to embryo attachment [43]. Similarly, miR-142 increases in the porcine mesometrial endometrium between days 12 and 15 and is more abundant at the mesometrial than at the anti-mesometrial side on day 15, precisely where conceptus attachment occurs [44]. In our study, however, both miRNAs showed an embryonic-associated distribution, being detected in EVs released by both UF-P and BL but absent in UF-C. Their detection in EVs released by embryos produced entirely *in vitro*, which had never been exposed to the maternal reproductive tract, further supports the capacity of the embryo to release these miRNAs independently of maternal exposure. Together, these findings raise the intriguing possibility that embryo-derived EVs may deliver miR-132 and miR-142 to the maternal environment, where they could contribute to the molecular remodeling that precedes conceptus attachment. Such embryo-to-endometrium EV transfer is biologically plausible, as embryo-derived EVs have been shown to be internalized by endometrial cells in humans and cattle and to induce changes in endometrial gene expression [11, 45].

The most distinctive finding, however, was the identification of 16 interaction-induced miRNAs that were present exclusively in EVs from UF-P and absent from both UF-C and BL groups. This pattern suggests that interaction between the embryo and the maternal tract generates an EV-associated miRNA profile that is distinct from the sum of the two compartments considered separately. Previous studies have shown that uterine EVs collected during the peri-implantation period can be internalized by primary porcine trophoblast cells and induce transcriptomic and functional changes affecting proliferation, migration and invasion [36]. Similarly, endometrium-derived EVs have been shown to influence porcine embryo attachment and survival *in vitro* [46], Guzewska et al. demonstrated that signals produced by the porcine conceptus can regulate the EV secretory machinery of the maternal endometrium, suggesting that embryonic signals can reshape the capacity of maternal epithelial cells to generate EVs [47].

We selected 10 interaction-induced miRNAs (miR-136, miR-155, miR-181d, miR-193a, miR-769, miR-29c, miR-331, miR-339, miR-885 and miR-374b) that collectively yielded 4,819 unique predicted targets, with more than 1,000 genes targeted by at least two miRNAs and 190 by at least three. Their predicted targets were widely represented in Wnt, TGF-β, PI3K, PDGF, FGF, integrin, interleukin, inflammatory, apoptotic and angiogenic pathways, several of which were significantly overrepresented. These processes encompass many of the cellular changes required on both sides of the interface, including

trophoblast growth and survival, epithelial remodeling, adhesion, immune adaptation and vascular preparation [3, 37, 48, 49]. miR-155 is particularly illustrative of this context-dependent regulation. It has previously been identified in porcine endometrium-derived EVs and shown experimentally to influence embryo attachment and apoptosis, with excessive miR-155 impairing embryo attachment *in vitro* [46]. Additionally, in human endometrial epithelial cells, increased miR-29c reduces adhesive capacity through downregulation of *COL4A1*, indicating that precise regulation of this miRNA is important for the acquisition of a receptive phenotype [50].

In addition, differential abundance analysis showed that the EV-associated miRNA repertoire changed among the three experimental groups. The most pronounced pregnancy-associated change between uterine EV populations involved miR-92b, which was markedly less abundant in UF-P than in UF-C. Hua et al. showed that miR-92b is differentially represented in uterine-fluid EVs during the implantation period and that EV-mediated transfer of miR-92b from porcine endometrial epithelial cells to trophoblast cells promotes proliferation, migration and adhesion through direct targeting of *TSC1* and *DKK3* [22]. The lower abundance observed in UF-P on day 6 therefore suggests that regulation of this miRNA begins considerably earlier than the implantation period.

The much larger differences observed between uterine-fluid EVs and blastocyst-derived EVs further support the existence of source-specific miRNA cargo. Several of the most strongly enriched miRNAs in uterine EVs, including miR-10a, miR-30d, miR-320a and miR-423, have previously been associated with the porcine endometrium during pregnancy and implantation [35, 51, 52]. miR-10a is particularly interesting because Wessels et al. identified it predominantly on the maternal side of the porcine maternal-fetal interface and associated elevated endometrial miR-10a with sites of spontaneous conceptus loss, indicating that its biological significance may depend on tightly controlled abundance [51]. Conversely, several miRNAs were substantially more abundant in BL-derived EVs than in uterine-fluid EVs, such as miR-192. In pigs, serum exosomal miR-192 is increased during early pregnancy and has been proposed as a pregnancy biomarker; functional experiments showed that miR-192 directly targets *ITGA4*, while subsequent analyses in porcine endometrial epithelial cells linked miR-192 with PI3K-AKT, MAPK and mTOR signaling [53, 54]. Our finding that miR-192 is enriched in EVs released by BL raises the possibility that the embryo may contribute to the extracellular miR-192 signal observed during early pregnancy.

5. Conclusions

The day-6 porcine uterine EV-associated miRNA landscape consists of a shared molecular background complemented by maternal-associated, embryonic-associated and interaction-induced signatures. The demonstration that *in vivo*-derived blastocysts release EV-associated miRNAs provides direct evidence that the embryo contributes to the extracellular signaling environment of the uterus, while the appearance of a distinct interaction-induced profile indicates that this environment is actively reshaped once embryo and maternal tissues communicate. This molecular remodeling may represent an early

layer of embryo-maternal communication preceding maternal recognition of pregnancy and conceptus attachment.

Abbreviations

BL
Blastocyst
BSA
Bovine serum albumin
COCs
Cumulus–oocyte complexes
Cryo-EM
Cryo-electron microscopy
DLS
Dynamic light scattering
EVs
Extracellular vesicles
FC
Fold change
FDR
False discovery rate
FSC
Forward scatter
GO
Gene Ontology
IGV
Integrative Genomics Viewer
IVC
In vitro culture
IVD
In vivo-derived
IVF
In vitro fertilization
IVM
In vitro maturation
IVP
In vitro-produced
PBS
Phosphate-buffered saline
PCA

Principal component analysis
PCR
Polymerase chain reaction
PVA
Polyvinyl alcohol
SRA
Sequence Read Archive
SSC
Side scatter
TEM
Transmission electron microscopy
UF
Uterine fluid
UF-C
Uterine fluid from cyclic non-pregnant sows
UF-P
Uterine fluid from pregnant sows

Declarations

Ethics approval and consent to participate

This study was conducted in accordance with the ARRIVE (Animal Research: Reporting of In Vivo Experiments) guidelines and was approved by the Ministry of Livestock, Fisheries and Aquaculture of the Region of Murcia, Spain (Approval No. A13230503).

Consent for publication

Not applicable.

Competing interests

The authors declare that they have no competing interests.

Funding

This work was supported by the Spanish Ministry of Science, Innovation and Universities (MICIU) and the State Research Agency (AEI/10.13039/501100011033), co-funded by the European Regional Development Fund (ERDF/EU), under projects PID2022-137645OB-I00 and PID2023-150622OA-100. The funding bodies had no role in the study design, data collection, analysis or interpretation, or in the writing of the manuscript.

Author Contribution

DG-C: Conceptualization, Methodology, Writing-original draft. CGC-G: Methodology, Writing-review & editing. PB-C: Methodology, Writing-review & editing. AL-J: Methodology, Writing-review & editing. MG-C: Methodology, Writing-review & editing. MAG: Methodology, Writing-review & editing. CC: Methodology, Writing-review & editing. IP: Methodology, Writing-review & editing. EAM: Methodology, Writing-review & editing, Supervision, Funding acquisition, Project administration. CAM-S: Conceptualization, Methodology, Writing-original draft, Supervision, Funding acquisition, Project administration.All authors read and approved the final manuscript.

Acknowledgement

The authors thank the staff of Agropor SA piggery (Murcia, Spain) for their valuable assistance with animal care and herd management, and the staff of the local slaughterhouse (Comarán S.L., Madrid, Spain) for providing ovaries used in this study.

Data Availability

The small RNA sequencing data generated in this study have been deposited in the NCBI Sequence Read Archive (SRA) under BioProject accession number PRJNA1544457 (https://www.ncbi.nlm.nih.gov/bioproject/PRJNA1544457).

References

1. Kölle S, Hughes B, Steele H. Early embryo-maternal communication in the oviduct: A review. Mol Reprod Dev. 2020;87:650–62. https://doi.org/10.1002/mrd.23352.
2. Velazquez MA, Idriss A, Chavatte-Palmer P, Fleming TP. The mammalian preimplantation embryo: Its role in the environmental programming of postnatal health and performance. Anim Reprod Sci. 2023;256:107321. https://doi.org/10.1016/j.anireprosci.2023.107321.
3. Waclawik A, Kaczmarek MM, Blitek A, Kaczynski P, Ziecik AJ. Embryo-maternal dialogue during pregnancy establishment and implantation in the pig. Mol Reprod Dev. 2017;84:842–55. https://doi.org/10.1002/mrd.22835.
4. Garcia-Canovas M, Parrilla I, Cuello C, Gil MA, Martinez EA. Swine in vitro embryo production: Potential, challenges, and advances. Anim Reprod Sci. 2024;270:107600. https://doi.org/10.1016/j.anireprosci.2024.107600.
5. Van Niel G, D'Angelo G, Raposo G. Shedding light on the cell biology of extracellular vesicles. Nat Rev Mol Cell Biol. 2018;19:213–28. https://doi.org/10.1038/nrm.2017.125.
6. Barranco I, Almiñana C, Parra A, Martínez-Diaz P, Lucas X, Bauersachs S, et al. RNA profiles differ between small and large extracellular vesicle subsets isolated from porcine seminal plasma. BMC

Genomics. 2024;25:1250. https://doi.org/10.1186/s12864-024-11167-4.

7. Godakumara K, Dissanayake K, Hasan MM, Kodithuwakku SP, Fazeli A. Role of extracellular vesicles in intercellular communication during reproduction. Reprod Domest Anim. 2022;57(Suppl 5):14–21. https://doi.org/10.1111/rda.14205.
8. Mazzarella R, Cajas YN, Martínez MEG, Rizos D. Extracellular vesicles: emerging paradigms in bovine embryo-maternal communication. Anim Reprod. 2024;21:e20240065. https://doi.org/10.1590/1984-3143-ar2024-0065.
9. Travaglione A, De Gregorio V, Candela A, Genovese V, Cimmino M, Cañón-Beltrán K, et al. Bovine oviductal and uterine extracellular vesicles enhance blastocyst development in confined individual embryo culture. J Assist Reprod Genet. 2026;43:1921–34. https://doi.org/10.1007/s10815-026-03903-4.
10. Bridi A, Andrade GM, del Collado M, Sangalli JR, de Ávila ACFCM, Motta IG, et al. Small extracellular vesicles derived from in vivo- or in vitro-produced bovine blastocysts have different miRNAs profiles—Implications for embryo-maternal recognition. Mol Reprod Dev. 2021;88:628–43. https://doi.org/10.1002/mrd.23527.
11. Aguilera C, Velásquez AE, Gutierrez-Reinoso MA, Wong YS, Melo-Baez B, Cabezas J et al. Extracellular Vesicles Secreted by Pre-Hatching Bovine Embryos Produced In Vitro and In Vivo Alter the Expression of IFNtau-Stimulated Genes in Bovine Endometrial Cells. Int J Mol Sci. 2023;24:7438. https://doi.org/10.3390/ijms24087438
12. Melo-Báez B, Mellisho EA, Wong YS, Cabezas J, Caamaño D, Aguilera C, et al. Bovine embryos release extracellular vesicles with differential miRNA signature during the compaction and blastulation stages. Reprod Biol. 2023;23:100725. https://doi.org/10.1016/j.repbio.2022.100725.
13. Kim J, Lee J, Lee TB, Jun JH. Embryotrophic effects of extracellular vesicles derived from outgrowth embryos in pre- and peri-implantation embryonic development in mice. Mol Reprod Dev. 2019;86:187–96. https://doi.org/10.1002/mrd.23093.
14. Simon B, Bolumar D, Amadoz A, Jimenez-Almazán J, Valbuena D, Vilella F, et al. Identification and Characterization of Extracellular Vesicles and Its DNA Cargo Secreted During Murine Embryo Development. Genes (Basel). 2020;11:203. https://doi.org/10.3390/genes11020203.
15. Boom G, Jordan V, Chamley LW, Cree L. Embryo-derived extracellular vesicles and their potential as biomarkers for embryo quality during IVF: a systematic review. Hum Reprod Update. 2026;32:613–36. https://doi.org/10.1093/humupd/dmag014.
16. Burns GW, Brooks KE, Spencer TE. Extracellular vesicles originate from the conceptus and uterus during early pregnancy in sheep. Biol Reprod. 2016;94:56. https://doi.org/10.1095/biolreprod.115.134973.
17. Saadeldin IM, Kim SJ, Choi YB, Lee BC. Improvement of cloned embryos development by co-culturing with parthenotes: A possible role of exosomes/microvesicles for embryos paracrine communication. Cell Reprogram. 2014;16:223–34. https://doi.org/10.1089/cell.2014.0003.

18. Gascon-Collado D, Blanco-Cueto P, Cabrera-Gómez CG, Tan A, Zhu J, Li J, et al. Embryo-derived extracellular vesicle miRNA cargo reflects developmental competence in porcine in vitro-produced embryos. Theriogenology. 2027;268:118236. https://doi.org/10.1016/j.theriogenology.2026.118236.
19. Krawczynski K, Najmula J, Bauersachs S, Kaczmarek MM. MicroRNAome of porcine conceptuses and trophoblasts: Expression profile of microRNAs and their potential to regulate genes crucial for establishment of pregnancy. Biol Reprod. 2015;92:21. https://doi.org/10.1095/biolreprod.114.123588.
20. Szuszkiewicz J, Nitkiewicz A, Drzewiecka K, Kaczmarek MM. miR-26a-5p and miR-125b-5p affect trophoblast genes and cell functions important during early pregnancy†. Biol Reprod. 2022;107:590–604. https://doi.org/10.1093/biolre/ioac071.
21. Ding Y, Hu Q, Gan J, Zang X, Gu T, Wu Z, et al. Effect of miR-143-3p from Extracellular Vesicles of Porcine Uterine Luminal Fluid on Porcine Trophoblast Cells. Anim (Basel). 2022;12:3402. https://doi.org/10.3390/ani12233402.
22. Hua R, Liu Q, Lian W, Kang TT, Gao D, Huang C, et al. Extracellular vesicles derived from endometrial epithelial cells deliver exogenous miR-92b-3p to affect the function of embryonic trophoblast cells via targeting TSC1 and DKK3. Reprod Biol Endocrinol. 2022;20:152. https://doi.org/10.1186/s12958-022-01023-z.
23. Funahashi H, Ekwall H, Rodriguez-Martinez H. Zona reaction in porcine oocytes fertilized in vivo and in vitro as seen with scanning electron microscopy. Biol Reprod. 2000;63:1437–42. https://doi.org/10.1095/biolreprod63.5.1437.
24. Gil MA, Nohalez A, Martinez CA, Ake-Villanueva JR, Centurion-Castro F, Maside C, et al. Effects of meiotic inhibitors and gonadotrophins on porcine oocytes in vitro maturation, fertilization and development. Reprod Domest Anim. 2017;52:873–80. https://doi.org/10.1111/rda.12993.
25. Welsh JA, Goberdhan DCI, O'Driscoll L, Buzas EI, Blenkiron C, Bussolati B, et al. Minimal information for studies of extracellular vesicles (MISEV2023): from basic to advanced approaches. J Extracell Vesicles. 2024;13:e12404. https://doi.org/10.1002/jev2.12404.
26. Robinson JT, Thorvaldsdóttir H, Winckler W, Guttman M, Lander ES, Getz G, et al. Integrative genomics viewer. Nat Biotechnol. 2011;29:24–6. https://doi.org/10.1038/nbt.1754.
27. Aparicio-Puerta E, Hirsch P, Schmartz GP, Kern F, Fehlmann T, Keller A. miEAA 2023: updates, new functional microRNA sets and improved enrichment visualizations. Nucleic Acids Res. 2023;51:W319–25. https://doi.org/10.1093/nar/gkad392.
28. Kozomara A, Birgaoanu M, Griffiths-Jones S. miRBase: from microRNA sequences to function. Nucleic Acids Res. 2019;47:D155–62. https://doi.org/10.1093/nar/gky1141.
29. Agarwal V, Bell GW, Nam JW, Bartel DP. Predicting effective microRNA target sites in mammalian mRNAs. eLife. 2015;4:e05005. https://doi.org/10.7554/eLife.05005.
30. Mi H, Muruganujan A, Casagrande JT, Thomas PD. Large-scale gene function analysis with the PANTHER classification system. Nat Protoc. 2013;8:1551–66. https://doi.org/10.1038/nprot.2013.092.

31. Szklarczyk D, Nastou K, Koutrouli M, Kirsch R, Mehryary F, Hachilif R, et al. The STRING database in 2025: protein networks with directionality of regulation. Nucleic Acids Res. 2025;53:D730–7. https://doi.org/10.1093/nar/gkae1113.
32. Geisert RD, Bazer FW, Lucas CG, Pfeiffer CA, Meyer AE, Sullivan R, et al. Maternal recognition of pregnancy in the pig: A servomechanism involving sex steroids, cytokines and prostaglandins. Anim Reprod Sci. 2024;264:107452. https://doi.org/10.1016/j.anireprosci.2024.107452.
33. Ziecik A, Waclawik A, Kaczmarek M, Blitek A, Jalali BM, Andronowska A. Mechanisms for the Establishment of Pregnancy in the Pig. Reprod Domest Anim. 2011;46(Suppl 3):31–41. https://doi.org/10.1111/j.1439-0531.2011.01843.x.
34. Geisert RD, Johnson GA, Burghardt RC. Implantation and establishment of pregnancy in the pig. Adv Anat Embryol Cell Biol. 2015;216:137–63. https://doi.org/10.1007/978-3-319-15856-3_8.
35. Su L, Liu R, Cheng W, Zhu M, Li X, Zhao S, et al. Expression Patterns of MicroRNAs in Porcine Endometrium and Their Potential Roles in Embryo Implantation and Placentation. PLoS ONE. 2014;9:e87867. https://doi.org/10.1371/journal.pone.0087867.
36. Szuszkiewicz J, Myszczynski K, Reliszko ZP, Heifetz Y, Kaczmarek MM. Early steps of embryo implantation are regulated by exchange of extracellular vesicles between the embryo and the endometrium. FASEB J. 2022;36:e22450. https://doi.org/10.1096/fj.202200677r.
37. Geisert RD, Lucy MC, Whyte JJ, Ross JW, Mathew DJ. Cytokines from the pig conceptus: roles in conceptus development in pigs. J Anim Sci Biotechnol. 2014;5:51. https://doi.org/10.1186/2049-1891-5-51.
38. Johnson GA, Burghardt RC, Bazer FW. Osteopontin: a leading candidate adhesion molecule for implantation in pigs and sheep. J Anim Sci Biotechnol. 2014;5:56. https://doi.org/10.1186/2049-1891-5-56.
39. Gupta A, Dekaney CM, Bazer FW, Madrigal MM, Jaeger LA. Beta Transforming Growth Factors (TGFβ) at the Porcine Conceptus-Maternal Interface. Part II: Uterine TGFβ Bioactivity and Expression of Immunoreactive TGFβs (TGFβ1, TGFβ2, and TGFβ3) and Their Receptors (Type I and Type II). Biol Reprod. 1998;59:911–7. https://doi.org/10.1095/biolreprod59.4.911.
40. Massuto DA, Kneese EC, Johnson GA, Burghardt RC, Hooper RN, Ing NH, et al. Transforming growth factor beta (TGFB) signaling is activated during porcine implantation: proposed role for latency-associated peptide interactions with integrins at the conceptus–maternal interface. Reproduction. 2010;139:465–78. https://doi.org/10.1530/rep-09-0447.
41. Ka H, Al-Ramadan S, Erikson DW, Johnson GA, Burghardt RC, Spencer TE, et al. Regulation of Expression of Fibroblast Growth Factor 7 in the Pig Uterus by Progesterone and Estradiol. Biol Reprod. 2007;77:172–80. https://doi.org/10.1095/biolreprod.106.056309.
42. Rodriguez-Martinez H, Persson E, Hurst M, Stanchev P. Immunohistochemical Localization of Platelet-Derived Growth Factor Receptors in the Porcine Uterus During the Oestrous Cycle and Pregnancy. Zentralbl Veterinarmed A. 1992;39:1–10. https://doi.org/10.1111/j.1439-0442.1992.tb00151.x.

43. Wang Y, Hu T, Wu L, Liu X, Xue S, Lei M. Identification of non-coding and coding RNAs in porcine endometrium. Genomics. 2017;109:43–50. https://doi.org/10.1016/j.ygeno.2016.11.007.
44. Huang J, Yang Y, Tian M, Deng D, Yu M. Spatial Transcriptomic and miRNA Analyses Revealed Genes Involved in the Mesometrial-Biased Implantation in Pigs. Genes (Basel). 2019;10:808. https://doi.org/10.3390/genes10100808.
45. Giacomini E, Vago R, Sanchez AM, Podini P, Zarovni N, Murdica V, et al. Secretome of in vitro cultured human embryos contains extracellular vesicles that are uptaken by the maternal side. Sci Rep. 2017;7:5210. https://doi.org/10.1038/s41598-017-05549-w.
46. Saadeldin IM, Tanga BM, Bang S, Seo C, Koo O, Yun SH, et al. ROCK Inhibitor (Y-27632) Abolishes the Negative Impacts of miR-155 in the Endometrium-Derived Extracellular Vesicles and Supports Embryo Attachment. Cells. 2022;11:3178. https://doi.org/10.3390/cells11193178.
47. Guzewska MM, Myszczynski K, Heifetz Y, Kaczmarek MM. Embryonic signals mediate extracellular vesicle biogenesis and trafficking at the embryo–maternal interface. Cell Commun Signal. 2023;21:210. https://doi.org/10.1186/s12964-023-01221-1.
48. Kridli RT, Khalaj K, Bidarimath M, Tayade C. Placentation, maternal–fetal interface, and conceptus loss in swine. Theriogenology. 2016;85:135–44. https://doi.org/10.1016/j.theriogenology.2015.08.001.
49. Kaczynski P, Goryszewska-Szczurek E, Baryla M, Waclawik A. Novel insights into conceptus–maternal signaling during pregnancy establishment in pigs. Mol Reprod Dev. 2023;90:658–72. https://doi.org/10.1002/mrd.23567.
50. Griffiths M, Van Sinderen M, Rainczuk K, Dimitriadis E. miR-29c overexpression and COL4A1 downregulation in infertile human endometrium reduces endometrial epithelial cell adhesive capacity in vitro implying roles in receptivity. Sci Rep. 2019;9:8644. https://doi.org/10.1038/s41598-019-45155-6.
51. Wessels JM, Edwards AK, Khalaj K, Kridli RT, Bidarimath M, Tayade C. The microRNAome of pregnancy: deciphering miRNA networks at the maternal-fetal interface. PLoS ONE. 2013;8:e72264. https://doi.org/10.1371/journal.pone.0072264.
52. Hong L, Liu R, Qiao X, Wang X, Wang S, Li J, et al. Differential microRNA Expression in Porcine Endometrium Involved in Remodeling and Angiogenesis That Contributes to Embryonic Implantation. Front Genet. 2019;10:661. https://doi.org/10.3389/fgene.2019.00661.
53. Gao R, Li Q, Qiu M, Xie S, Sun X, Huang T. Serum exosomal miR-192 serves as a potential detective biomarker for early pregnancy screening in sows. Anim Biosci. 2023;36:1336–49. https://doi.org/10.5713/ab.22.0422.
54. Li Q, Gao R, Chen Y, Xie S, Sun X, Gong H, et al. Identification of miR-192 target genes in porcine endometrial epithelial cells based on miRNA pull-down. Mol Biol Rep. 2023;50:4273–84. https://doi.org/10.1007/s11033-023-08349-w.

Figures

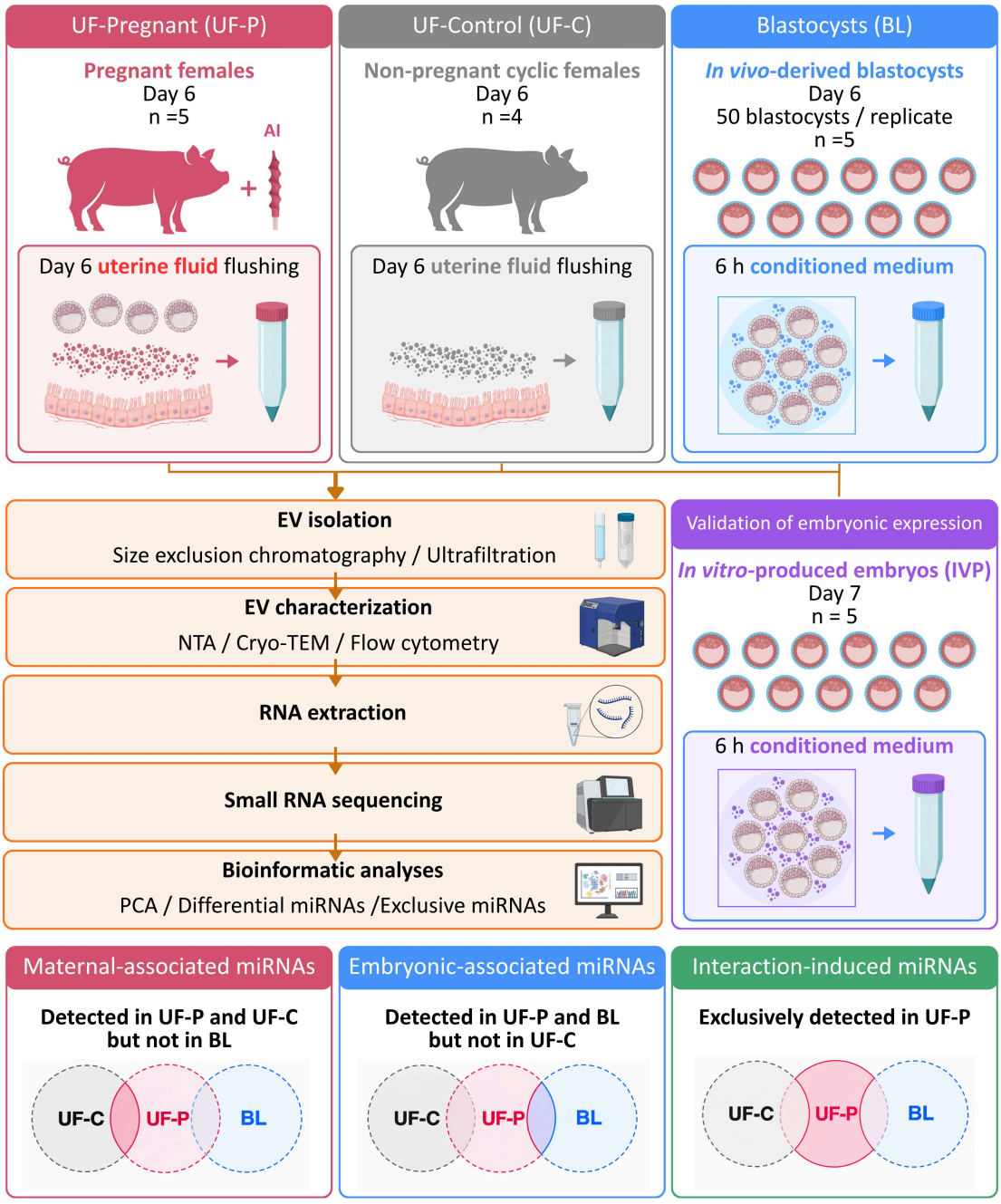


Figure 1

Schematic representation of the experimental design. Extracellular vesicles (EVs) were isolated from uterine fluid collected on day 6 from pregnant sows (UF-P, n = 5) and cyclic non-pregnant control sows (UF-C, n = 4), and from conditioned medium generated by culturing pools of 50 in vivo-derived day-6 blastocysts (BL, n = 5) for 6 h in protein-free medium. EVs were isolated by size-exclusion chromatography followed by ultrafiltration, characterized, and subjected to RNA extraction, small RNA

sequencing, and bioinformatic analyses. Based on their distribution across UF-P, UF-C, and BL samples, miRNAs were classified as maternal-associated (detected in UF-P and UF-C but not BL), embryonic-associated (detected in UF-P and BL but not UF-C), or interaction-induced (detected exclusively in UF-P). EVs released by in vitro-produced embryos (IVP, n = 5) were additionally analyzed to provide independent support for the embryonic origin of selected miRNAs.

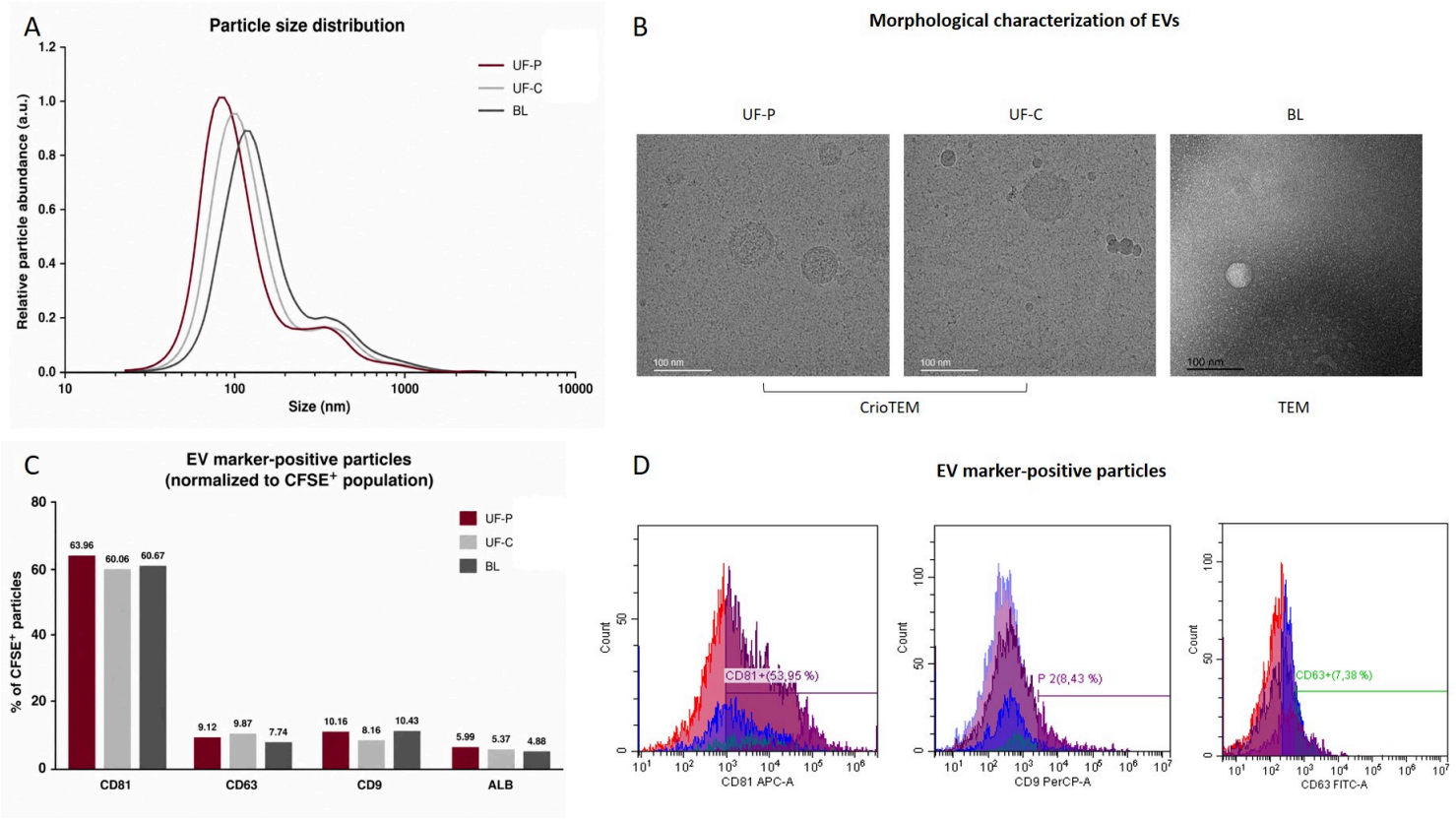


Figure 2

Characterization of extracellular vesicles (EVs) isolated from uterine fluid of pregnant (UF-Pregnant) and non-pregnant (UF-Control) sows, and in vivo-derived blastocysts (BL). (A) Particle size distribution profiles as determined by ZetaView. (B) Representative transmission electron microscopy (cryo-TEM/TEM) images of EVs isolated from uterine fluid of pregnant sows (UF-P), uterine fluid of cyclic control sows (UF-C), and blastocyst-conditioned medium (BL). (C) Flow cytometry quantification of EV-associated markers (CD81, CD63 and CD9) and albumin (ALB) expressed as the percentage of positive particles within the CFSE-positive population. (D) Representative flow cytometry histograms showing the detection of EV-associated markers in isolated EV preparations.

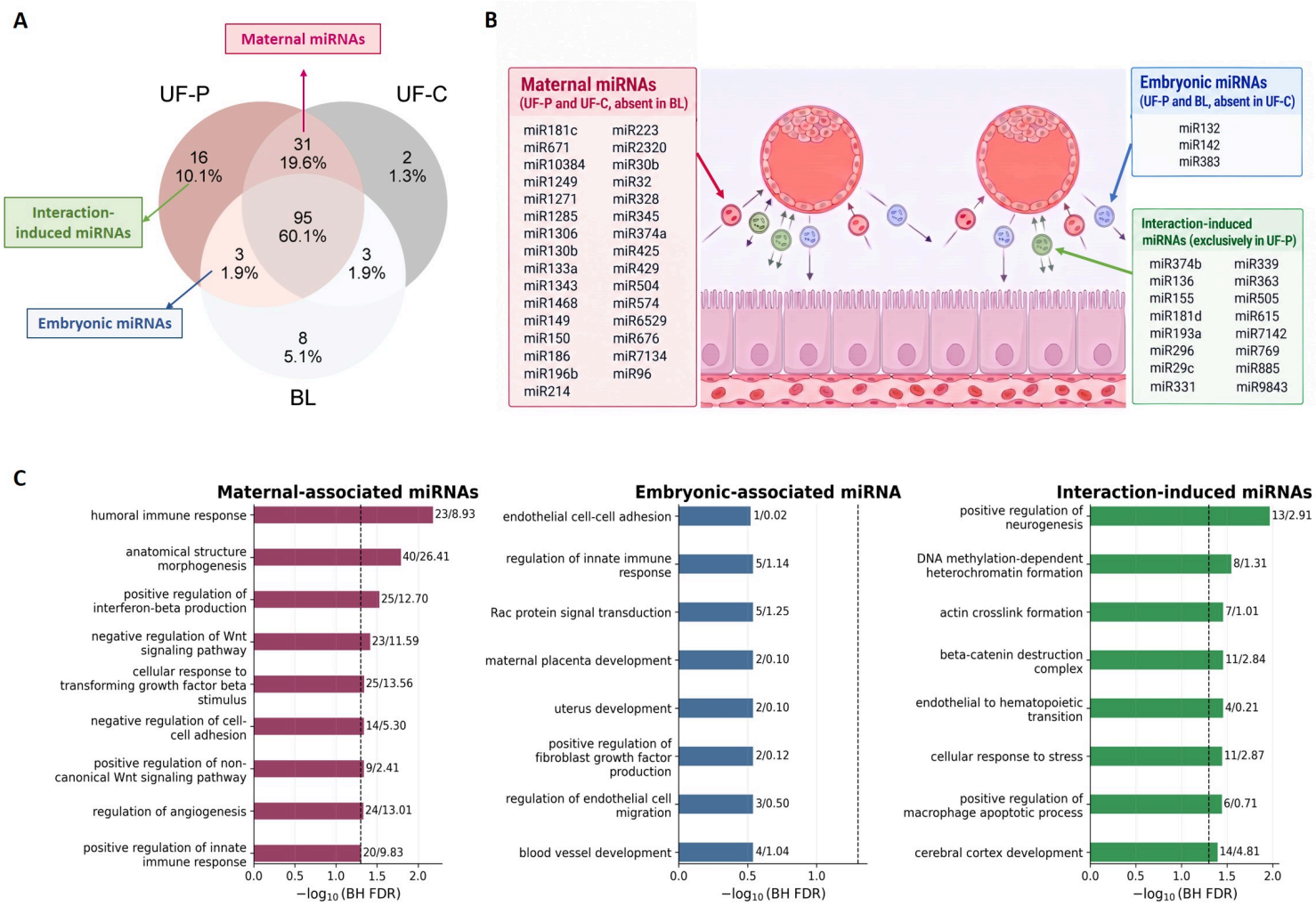


Figure 3

Distribution and functional characterization of extracellular vesicles (EVs)-associated miRNAs according to their potential contribution to embryo-maternal communication. (A) Venn diagram showing the distribution of miRNAs detected in EVs isolated from uterine fluid (UF) of pregnant sows (UF-P), UF of cyclic control sows (UF-C), and blastocyst-conditioned medium (BL). Numbers and percentages indicate miRNAs detected within each region relative to the total number of miRNAs identified across the three EV populations (n = 158). Based on their distribution, miRNAs detected in both UF-P and UF-C but absent from BL were classified as maternal-associated miRNAs (n = 31); those detected in UF-P and BL but absent from UF-C as embryonic-associated miRNAs (n = 3); and those exclusively detected in UF-P as interaction-induced miRNAs (n = 16). (B) Schematic representation of the proposed contribution of these miRNA signatures to EV-mediated communication within the uterine environment during early pregnancy. (C) Gene Ontology (GO) analysis of maternal-associated, embryonic-associated, and interaction-induced miRNA sets. Bars represent -log10-transformed Benjamini-Hochberg false discovery rate (BH FDR) values for selected GO terms.

A **Maternal-associated Target Genes**

Target-gene analysis	N	miRNA	Predicted targets
Maternal-associated miRNAs detected	31	miR-30b-5p	1151
miRNAs with TargetScan analysis	10	miR-96-5p	947
All unique target genes	4220	miR-150-5p	168
Targets predicted by ≥2 miRNAs	1295	miR-130b-5p	801
Targets predicted by ≥3 miRNAs	364	miR-133a-3p	795
Targets predicted by ≥4 miRNAs	93	miR-181c-3p	715
Targets predicted by ≥5 miRNAs	17	miR-223-3p	321
Targets predicted by ≥6 miRNAs	5	miR-214-3p	117
		miR-149-5p	339
		miR-429-3p	640

B **Embryonic-associated Target Genes**

Target-gene analysis	N	miRNA	Predicted targets
Embryonic-associated miRNAs detected	3	miR-383-5p	1586
miRNAs with TargetScan analysis	3	miR-132-3p	321
All unique target genes	2182	miR-142-5p	362
Targets predicted by ≥2 miRNAs	83		
Targets predicted by ≥3 miRNAs	4		

C **Pathway Analysis**

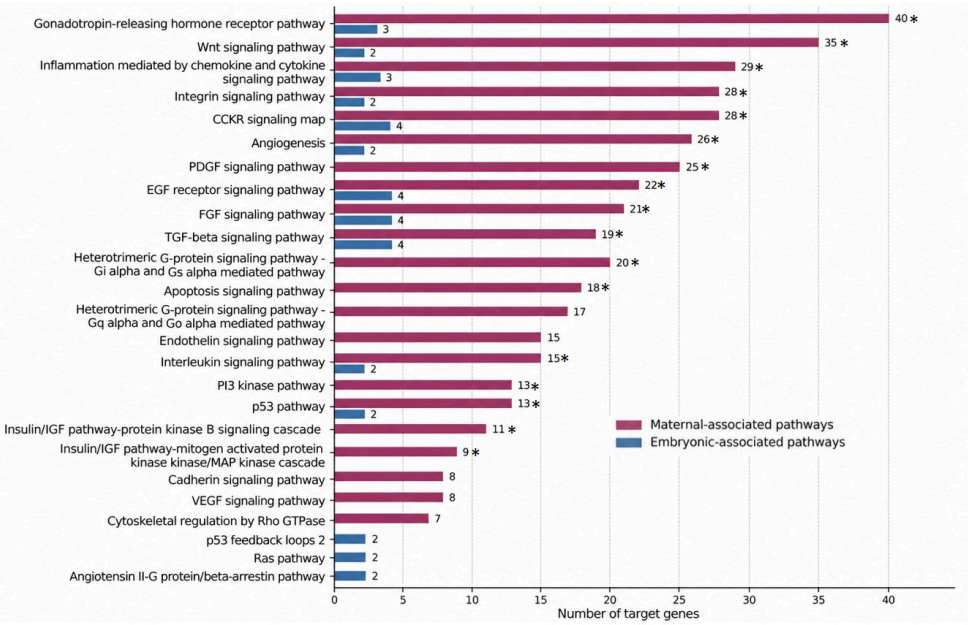


Figure 4

Target convergence and pathway analysis of maternal- and embryonic-associated miRNAs. (A) Target-gene analysis of 10 selected maternal-associated miRNAs (expressed in extracellular vesicles (EVs) isolated from uterine fluid (UF) of pregnant sows (UF-P), and UF of cyclic control sows (UF-C), but absent in blastocyst-conditioned medium (BL)), and (B) Target-gene analysis of the 3 embryonic-associated miRNAs (expressed in UF-P and BL, but absent in UF-C), using TargetScan analysis. (C) Pathway distribution of convergent target genes (targeted by ≥ 2 miRNAs) from maternal-associated and embryonic-associated miRNAs. Bars indicate the number of convergent target genes assigned to each pathway. Maternal-associated pathways are shown in burgundy and embryonic-associated pathways in blue; where a pathway was represented in both signatures, both bars are shown. Asterisks indicate pathways significantly overrepresented among maternal-associated convergent targets after FDR correction (FDR < 0.05). No pathways remained significantly overrepresented in the embryonic-associated target set after FDR correction.

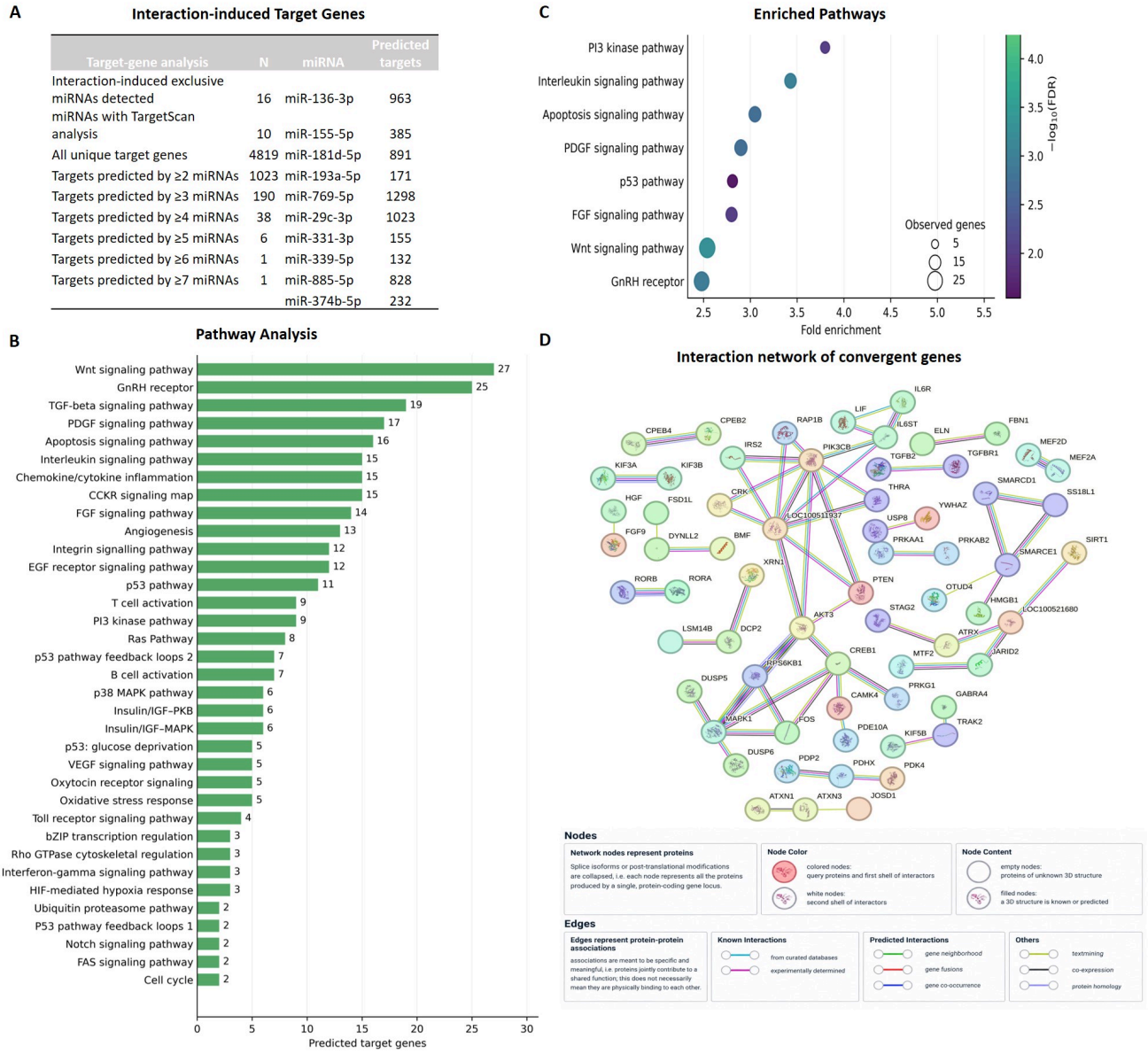


Figure 5

Target convergence, pathway analysis and gene interaction network of interaction-induced miRNAs. (A) Target-gene analysis of 10 selected interaction-induced miRNAs (expressed exclusively in extracellular vesicles (EVs) isolated from uterine fluid (UF) from pregnant sows (UF-P), and absent in UF of cyclic control sows (UF-C), and blastocyst-conditioned medium (BL)), using TargetScan analysis. (B) PANTHER pathway distribution of convergent target genes (targeted by ≥ 2 miRNAs). Bars indicate the number of predicted target genes assigned to each pathway. (C) Significantly overrepresented PANTHER pathways among convergent target genes. Bubble position indicates fold enrichment, bubble size represents the number of observed genes, and bubble color indicates enrichment significance as −log10(FDR). (D) STRING gene interaction network of convergent target genes predicted to be targeted by at least 3 interaction-induced miRNAs.

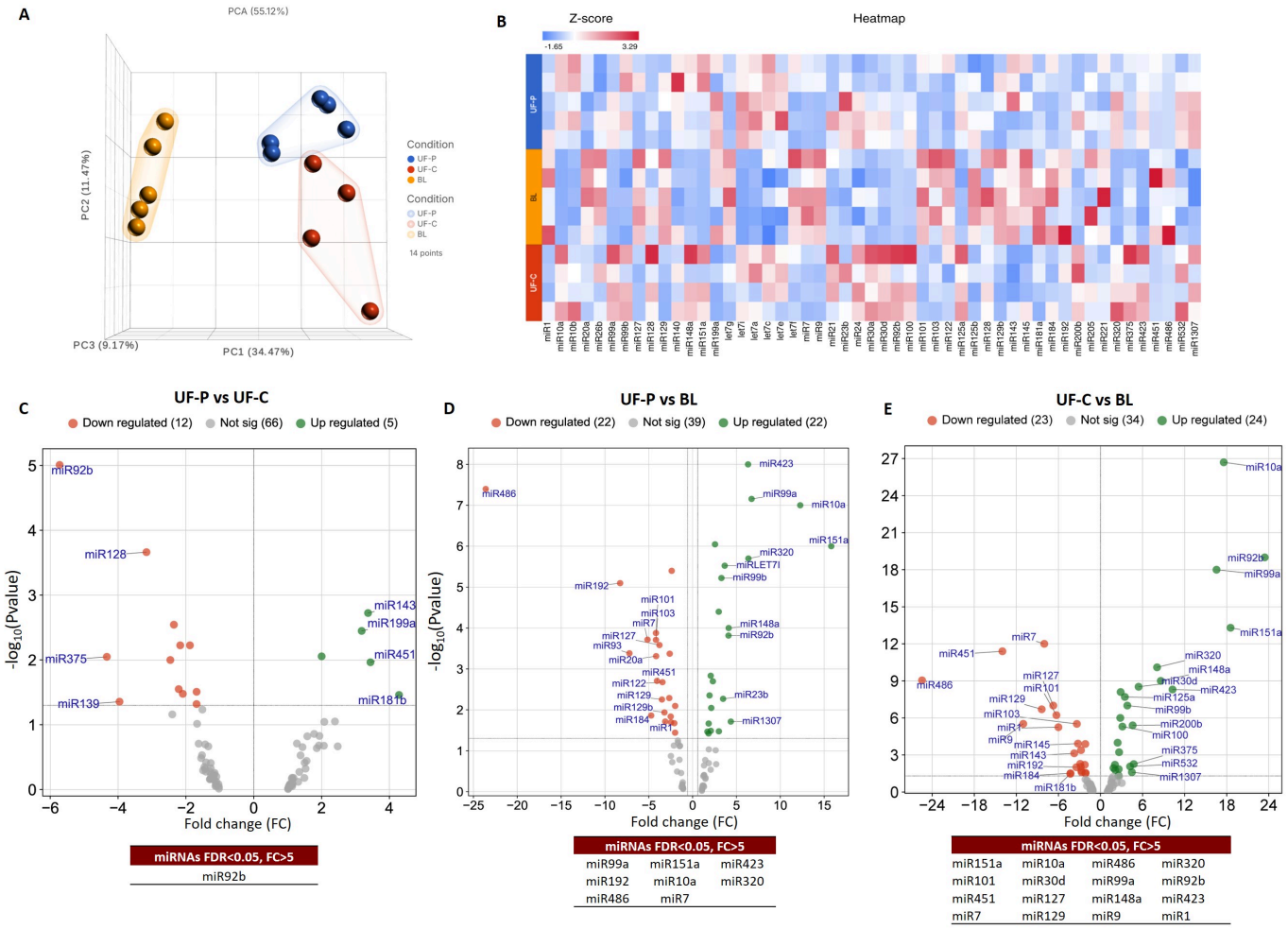


Figure 6

Global and differential miRNA profiles of extracellular vesicles (EVs) derived from uterine fluid (UF) of pregnant sows (UF-P), UF of cyclic control sows (UF-C), and blastocyst-conditioned medium (BL). (A) Principal component analysis (PCA) illustrates the distribution of samples according to their miRNA profiles in EVs isolated from all groups. (B) The heatmap shows miRNAs with FDR < 0.05 and |FC| > 1.5 in at least one pairwise comparison, illustrating their relative abundance across individual samples. (C-E) Volcano plots show pairwise differential miRNA expression between UF-P and UF-C, UF-P and BL, and UF-C and BL, respectively. Differentially expressed miRNAs were defined using P < 0.05 and |FC| > 1.5. Only miRNAs with |FC| > 3 are labelled in the volcano plots. Tables below each plot show miRNAs with |FC| > 5 that remained significant after multiple-testing correction (FDR < 0.05).

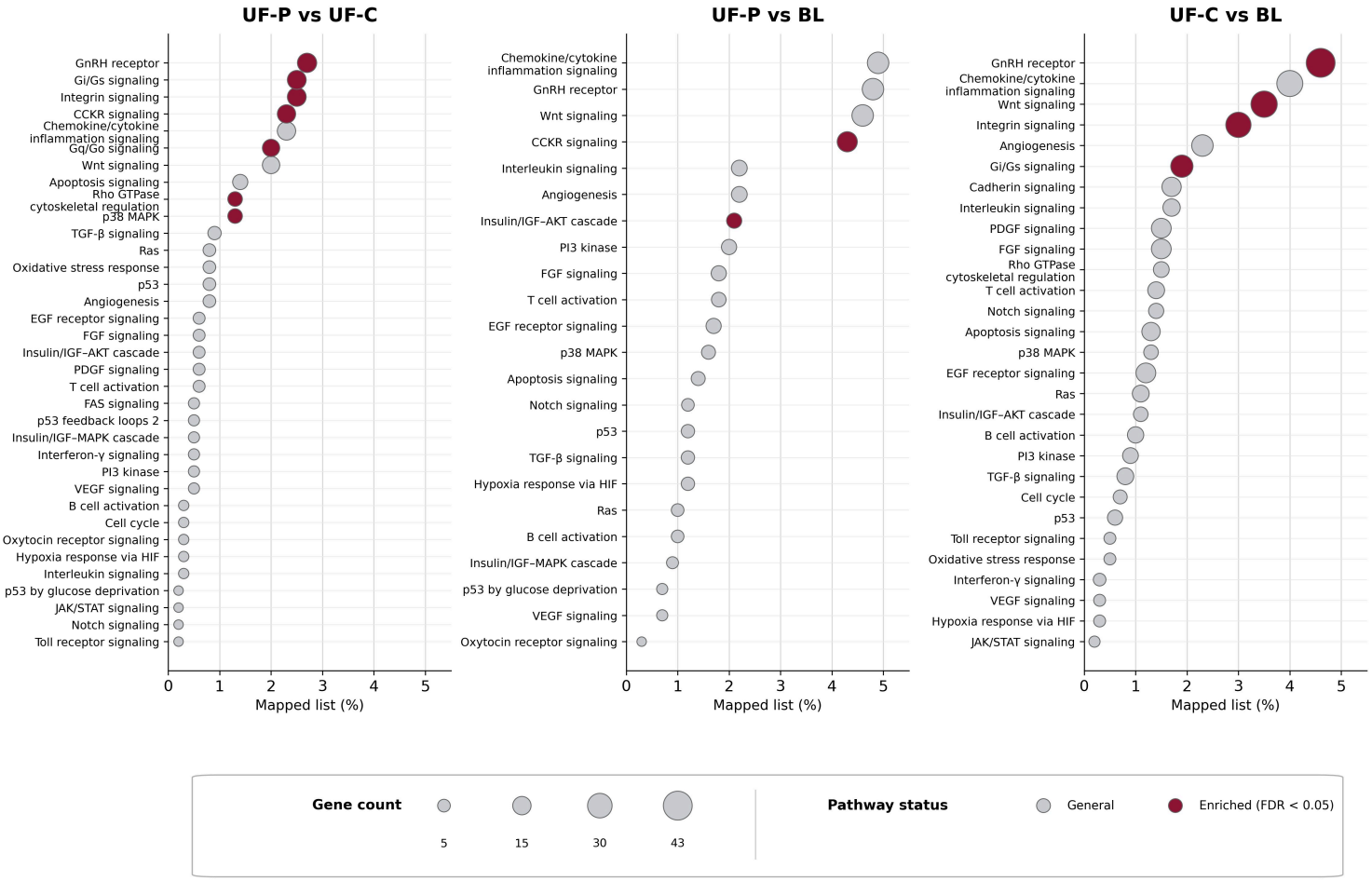


Figure 7

Pathway classification of predicted target genes associated with differentially abundant miRNAs detected in extracellular vesicles (EVs) isolated from uterine fluid (UF) of pregnant sows (UF-P), UF of cyclic control sows (UF-C), and blastocyst-conditioned medium (BL). For comparisons containing both up- and downregulated miRNAs, pathways detected in the two directional analyses were summarized within a single comparison. The x-axis represents the percentage of the mapped target list assigned to each pathway (Mapped list, %), whereas bubble size reflects the number of pathway-associated target-gene hits. Grey bubbles indicate selected biologically relevant pathways identified in the general classification, while burgundy bubbles denote pathways significantly overrepresented in the corresponding overrepresentation test (Fisher's exact test, FDR < 0.05).

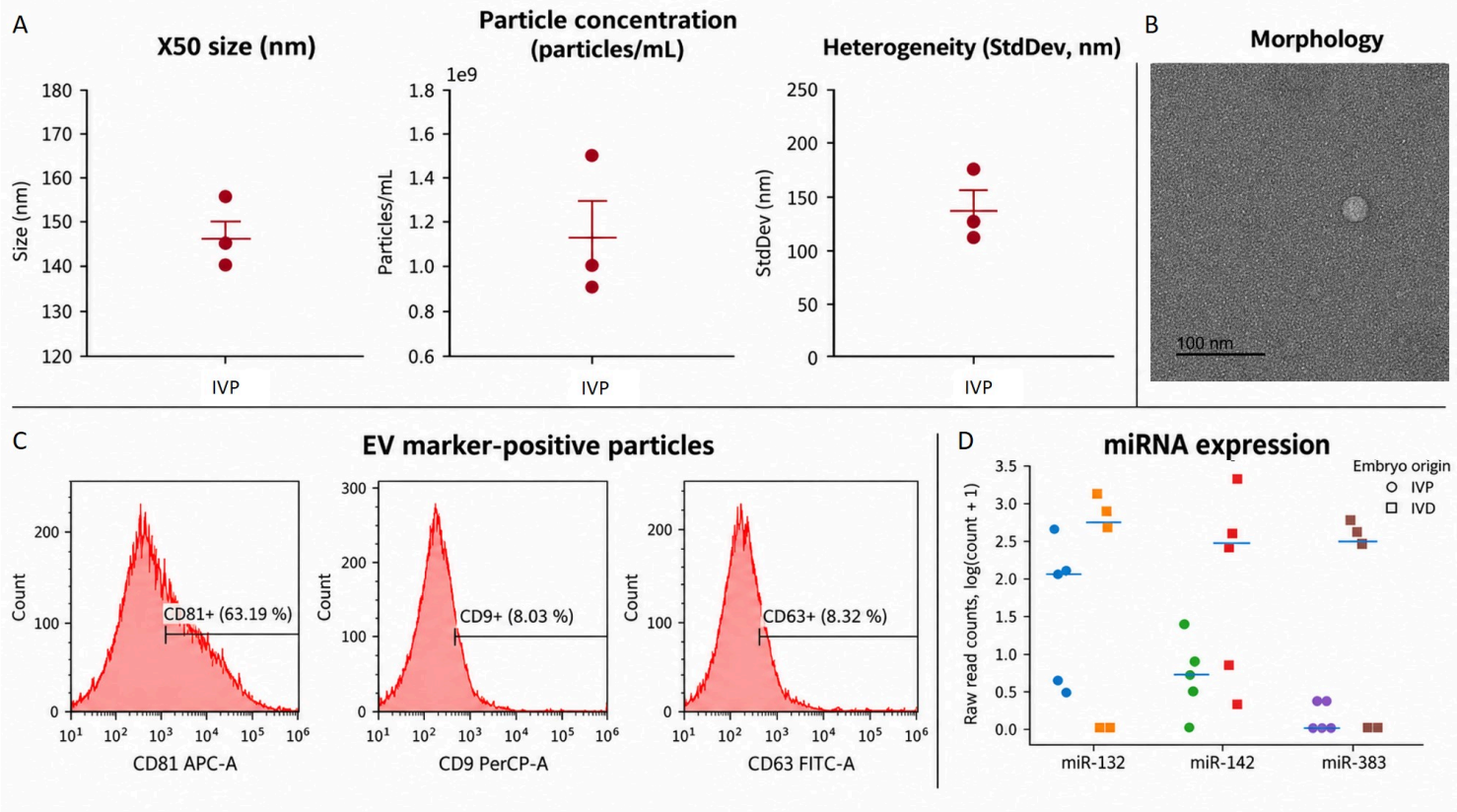


Figure 8

Characterization of extracellular vesicles (EVs) released by in vitro-produced (IVP) porcine embryos and detection of embryo-associated miRNAs in EVs from IVP and in vivo-derived (IVD) embryos. (A) EVs were characterized by particle size, particle concentration, and size heterogeneity, as determined by ZetaView. (B) Representative transmission electron microscopy (TEM) image of EVs isolated from IVP embryos. (C) Representative flow cytometry histograms showing the detection of EV-associated markers in isolated EV preparations. (D) Raw read counts of miR-132, miR-142 and miR-383 in EVs released by IVP embryos and IVV embryos. Each point represents one biological replicate (n = 5 per group). Circles indicate IVP embryos and squares indicate IVD embryos; horizontal lines represent the median. Raw read counts are displayed as log10(count + 1) to allow visualization across the wide range of detected abundances.

Supplementary Files

This is a list of supplementary files associated with this preprint. Click to download.

- Additionalfile1.xlsx
- Additionalfile2.xlsx
- Additionalfile3.xlsx